Scripta Materialia 111 (2016) 106–109

Contents lists available at ScienceDirect

Scripta Materialia

journal homepage: www.elsevier.com/locate/scriptamat

Plasma-enhanced atomic layer deposition of $BaTiO_3$

Peter Schindler [a,1], Yongmin Kim [a,1], Dickson Thian [b], Jihwan An [a,c,*], Fritz B. Prinz [a,d]

[a] Department of Mechanical Engineering, Stanford University, Stanford, CA 94305, USA
[b] Department of Applied Physics, Stanford University, Stanford, CA 94305, USA
[c] Manufacturing Systems and Design Engineering Programme, Seoul National University of Science and Technology, Seoul 139-743, South Korea
[d] Department of Materials Science and Engineering, Stanford University, Stanford, CA 94305, USA

ARTICLE INFO

Article history:
Received 23 July 2015
Accepted 23 August 2015
Available online 28 August 2015

Keywords:
High-*k* thin films
Atomic layer deposition (ALD)
Plasma-enhanced ALD
DRAM capacitor

ABSTRACT

Among high-*k* thin films, perovskite $BaTiO_3$ (BTO) is an attractive candidate due to its exceptionally high dielectric constant. In contrast to conventional atomic layer deposition (ALD), plasma-enhanced ALD (PEALD) has several advantages such as lower process temperature, improved film quality and the deposition of a wider spectrum of materials. We report the successful deposition of high-*k* BTO thin films by PEALD. Compositional, morphological, and crystallographic characterizations of PEALD BTO are presented. The electrical performance of PEALD BTO thin films as a function of Ba-to-Ti-ratio is shown. Slightly Ti-rich BTO has the lowest equivalent oxide thickness while Ba-rich films show the lowest leakage current.

© 2015 Acta Materialia Inc. Published by Elsevier Ltd. All rights reserved.

The use of high-*k* thin films that exhibit a low leakage current is essential in realizing dynamic random access memory (DRAM) capacitors with high charge storage density and long storage lifetime [1,2]. Among high-*k* thin films, perovskites such as $BaTiO_3$ (BTO), $SrTiO_3$ (STO), or $(Ba,Sr)TiO_3$ (BST) are attractive candidates due to their exceptionally high dielectric constants maintained even for thin films (>100) [2–7]. Recent development of DRAM structures have necessitated the down-scaling of features to smaller dimensions (<30 nm), i.e. higher aspect-ratios, for enhanced information storage densities. Therefore, the conformal coating of high-*k* thin films over the inner surface of high aspect-ratio trenches is of great importance.

In this regard, atomic layer deposition (ALD), which is dominated by unique self-limiting surface reactions, is an attractive tool to fabricate DRAM capacitors. ALD enables the deposition of conformal films over complex 3-dimensional geometries with precise thickness control. Additionally, one can minimize the thermal damage of the device in the process of the deposition due to the relatively low process temperature (<400 °C) during ALD [8]. Plasma-enhanced ALD (PEALD), in which excited species (such as ions and radicals) generated by a plasma are used to react with ligands of the precursor during the second half-step, has several advantages compared to the conventional thermal ALD [9]; for example, the highly reactive plasma species give more flexibility in processing conditions and materials properties. PEALD films are also known to possess higher density and less contamination originated from unreacted ligands, which potentially results in the lowered electrical leakage current of dielectric oxide films [9].

In this report, we demonstrate for the first time the successful deposition of PEALD BTO films using cyclopentadienyl(Cp*)-type barium precursor, $Ba(iPr_3Cp^*)_2$ (iPr_3Cp^* = 1,2,4-trisisopropyl-cyclo pentadienyl). The growth behaviors of the individual oxides (i.e., BaO and TiO_2) and of $BaTiO_3$ have been tested and the ALD growth-mode was confirmed. The detailed compositional, morphological, and crystallographic characteristics of the PEALD BTO are presented, and compared to those of thermal ALD BTO films previously reported [10]. PEALD of BTO films showed to result in more uniform and denser films with more crystallites dispersed in the amorphous BTO matrix, compared to thermal ALD BTO. Lastly, the electrical performance of PEALD BTO films is shown as a function of Ba-to-Ti cation ratio for the possible application in charge storage capacitors.

BTO films were deposited in a commercial PEALD reactor (FlexAl, Oxford Instruments). $Ba(^iPr_3Cp)_2$ (Air Liquide) and Ti $(OCH(CH_3)_2)_4$ (TTIP, Sigma Aldrich) were utilized as the Ba and Ti precursors, respectively. The precursor canisters of the Ba and Ti precursors were heated to 180 and 55 °C, respectively. Oxygen plasma was generated from an inductively coupled plasma system (plasma power, 250 W; operating pressure, 15 mTorr). The BaO PEALD process consisted of (i) Ba precursor injection (3 s) followed by (ii) Ba precursor exposure (60 s) to enhance diffusion and

* Corresponding author at: Manufacturing Systems and Design Engineering Programme, Seoul National University of Science and Technology, Seoul 139-743, South Korea.

E-mail address: jihwanan@seoultech.ac.kr (J. An).

[1] These authors contributed equally to this work.

http://dx.doi.org/10.1016/j.scriptamat.2015.08.026
1359-6462/© 2015 Acta Materialia Inc. Published by Elsevier Ltd. All rights reserved.

adsorption of the precursor molecules, (iii) precursor purging by Ar (60 s), (iv) plasma stabilization (2 s), (v) O_2 plasma injection (10 s) and (vi) Ar purging (2 s). In case of the TiO_2 PEALD process, (i) TTIP injection (5 s), (ii) precursor purging by Ar (5 s), (iii) plasma stabilization (2 s), (iv) O_2 plasma injection (3 s) and (v) Ar purging (2 s) were employed. The BTO films with different cation composition ratios ([Ti]/([Ba] + [Ti]) = 0.26–0.76) were fabricated by alternately depositing one BaO cycle and several TiO_2 cycles, which together form one super-cycle.

The film thickness (t_{BTO}), roughness and density were measured by X-ray reflectivity (XRR) measurements (X'Pert Pro, PANalytical). The film thickness was also confirmed by a spectroscopic ellipsometer (Woollam M2000). High-resolution transmission electron microscopy (HRTEM) at an acceleration voltage of 300 kV was employed to analyze the crystallization of the samples (FEI Titan ETEM 300 kV). The composition analysis was conducted by X-ray photoelectron spectroscopy (XPS, PHI VersaProbe Scanning XPS Microscope) with Al (Kα) radiation (1486 eV). Atomic force microscopy (AFM, JEOL 5200) was used to characterize the surface morphology of the films. For the electrical measurement, Pt/BTO/p-doped Si metal–insulator–semiconductor capacitors were fabricated using highly p-doped Si wafers (a sheet resistance of 0.008 Ω cm) as substrates and a DC-sputtered Pt (200 nm) film as the top electrode. The electrical properties, (i) capacitance at 1 kHz and (ii) current density–voltage (*J*–*V*) curves (0 to +2 V) were measured by an LCR meter (Agilent, model No. E4980A) and a Keithley SourceMeter (2636A), respectively. The detailed process to obtain dielectric constants of BTO (ε_{BTO}) as well as the equivalent oxide thickness (EOT), i.e. $t_{BTO}(3.9/\varepsilon_{BTO})$, were reported elsewhere [10–12].

We first investigated the basic ALD characteristics of the individual oxides BaO and TiO_2 in order to be able to deposit stoichiometric BTO. Fig. S1a and b show the growth per cycle (GPC) of BaO as a function of substrate temperature (200–350 °C) and Ba precursor pulse time, respectively. The GPC of PEALD BaO in the range of 250–300 °C was nearly constant at 0.25–0.26 nm/cycle with 4–7% non-uniformity on a 4-inch wafer. Furthermore, the GPC values of PEALD BaO at 250 °C were saturated with a precursor pulse time longer than 3 s. However, the GPC of BaO was significantly increased to 7.6 ± 0.02 nm/cycle at 350 °C. Similarly, the measured GPC values of PEALD TiO_2 were ~0.045 nm/cycle with 2% non-uniformity at substrate temperatures of 200–300 °C (Fig. S1c). Further, the GPC of PEALD TiO_2 showed to be saturated with a precursor pulse time greater than 3 s as seen in Fig. S1d.

The saturation of the GPC with increasing precursor pulse time (in the range of 250–300 °C) implies that the deposition of BaO using $Ba(^iPr_3Cp)_2$ and O_2 plasma lies within the ALD window. The high GPC even at a relatively low deposition temperature (250 °C) clearly shows the benefit of using oxygen plasma as an oxidant over water or ozone. Furthermore, the deposition at 250 °C is appropriate to sustain thermal stability of the Ti-alkoxide-type precursor, TTIP, a key parameter for TiO_2 ALD growth [13]. The significant increase in GPC of BaO at 350 °C may be ascribed to the partial decomposition of $Ba(iPr_3Cp)_2$ to smaller alkyl-substituted Cp* complexes [2]. Lee et al. [2,13] also reported the chemical vapor deposition like growth of SrO when $Sr(^iPr_3Cp)_2$ was initially supplied to fresh substrates which readily provide oxygen (e.g. IrO_2 and RuO_2). Hence, these substrates show to be unfavorable for depositing films with a uniform Ba-to-Ti ratio in the direction of growth. In our work, this is not the case due to higher bond dissociation energies of Si–O and Ti–O bonds over the Ba–O bond (bond dissociation energies Hf_{298} (kJ/mol); Si–O: 798; Ti–O: 662; Ba–O: 563) [14]. The observed GPC values of TiO_2 are consistent with the previously reported GPC values, 0.04–0.05 nm/cycle at similar deposition conditions [15]. These results imply that the ALD mode deposition of BTO, which is fabricated by repeating BaO and TiO_2 layers alternately, is possible at the temperature range where both of them show a constant GPC, i.e. 250–300 °C.

Fig. 1a shows the cation ratio ([Ti]/([Ba] + [Ti]) inside the film depending on the ALD cycle ratio (i.e., the number of TiO_2 cycles per one BaO cycle). The cation ratios were controllable by simply changing the Ba:Ti cycle ratio: the film becomes slightly Ba-rich ([Ti]/([Ba] + [Ti] = 0.48) when the Ba:Ti cycle ratio is 1:1, and becomes slightly Ti-rich ([Ti]/([Ba] + [Ti] = 0.52) when the cycle ratio is 1:2. Fig. 1b shows the GPC versus the Ba:Ti cycle ratio: the GPC per supercycle is increased with increasing number of Ti

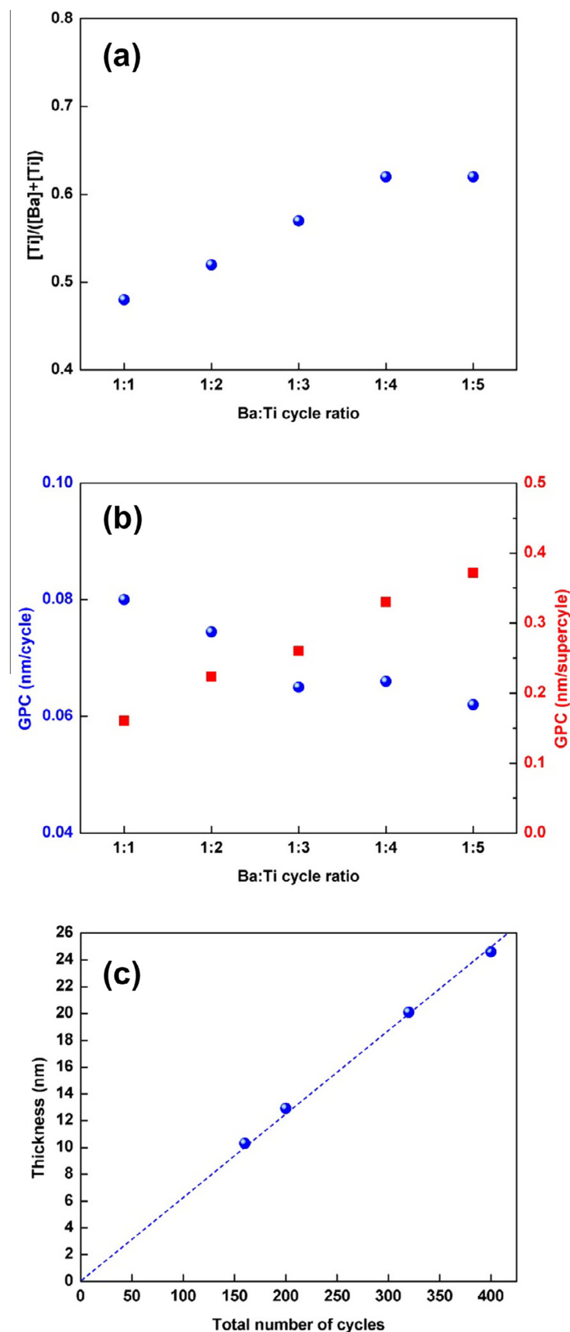

Fig. 1. (a) Composition ratio ([Ti]/([Ba] + [Ti])) and (b) GPC (blue for per individual cycles, red for per super-cycle) vs. Ba:Ti cycle ratio. (c) Thickness of the BTO film vs. total number of individual ALD cycles for BTO with the Ba:Ti cycle ratio of 1:3. (For interpretation of the references to color in this figure legend, the reader is referred to the web version of this article.)

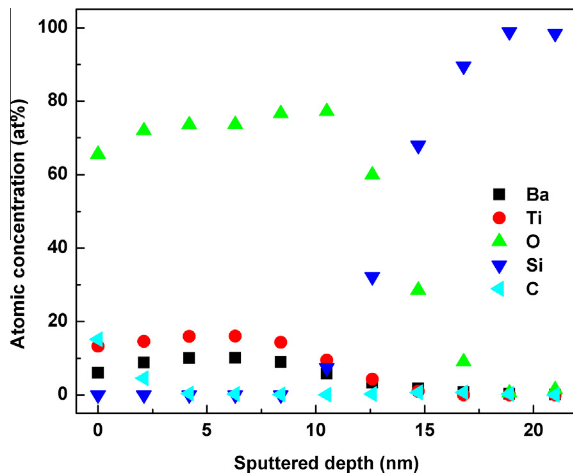

Fig. 2. XPS depth profile spectra of 12 nm-thick BTO (Ba:Ti cycle ratio of 1:3) deposited at 250 °C. Sputtering depth was calculated from sputtering time with the assumption of a sputtering rate of 7 nm/min.

cycles, however, the GPC per individual ALD cycle is monotonically decreased due to the small GPC of TiO_2 over BaO. At the Ba:Ti cycle ratio of 1:3, for example, the growth per individual cycle is measured to be 0.065 nm/cycle while the growth rate per super-cycle is 0.26 nm/cycle. At this deposition condition, the thickness of the BTO film increases linearly with increasing number of individual cycles (Fig. 1c).

We investigated the compositional, morphological and crystallographic properties of PEALD BTO (Ba:Ti cycle ratio of 1:3) deposited at 250 °C. Fig. 2 shows the XPS depth profile of a slightly Ti-rich BTO film with the cation ratio [Ti]/([Ba] + [Ti]) of 0.52 being uniform throughout the whole thickness (~12 nm). The carbon content was below the detection limit of XPS (<0.1 at.%) except for the top-most surface (<2 nm) resulting from the surface contamination. Surface morphology analysis by AFM (Fig. 3a) showed a root mean square roughness of 0.40 nm. Fig. 3b displays a cross-sectional TEM image of as-deposited PEALD BTO revealing small crystallites embedded in the amorphous matrix. The inset shows lattice spacings of 0.2 nm in agreement with (100) directions of cubic (a 0.394–0.403 nm), tetragonal (a 0.394–0.399 nm, c 0.399–0.404 nm), or rhombohedral (a 0.400 nm, θ 89.5°) [16]. A high film density of 5.0 g/cm^3 is measured by XRR for as-deposited PEALD BTO.

The XPS result shows that the ligand exchange reaction between the Ba and Ti precursors with the O_2 plasma (forming Ba–O and Ti–O bonds) occurs without the formation of any carbonate species that also has been observed by Lee et al. for thermal ALD STO deposited on a Ru substrate [2]. The roughness measured by AFM for PEALD BTO is smaller than that of thermal ALD BTO (0.63 nm) using H_2O as an oxidant with similar thickness [10]. One possible explanation for this is that the incident plasma species with an ion energy of ~20 eV effectively migrate surface atoms into sites with a high surface energy, eventually resulting in the lowered roughness without damaging the surface, supported by Takagi [17] As-deposited PEALD BTO shows 1–2 nm sized crystallites embedded in the amorphous matrix whereas thermal BTO appears to be completely amorphous [10]. Note that the crystallinity of as-deposited thermal ALD BTO films can be enhanced after being post-treated by O_2 plasma presumably due to the ion bombardment at the surface, providing the required energy for atomic rearrangement [10]. Similarly, during the deposition of PEALD BTO, O_2 plasma species with the primary object of oxidizing precursors activated the BTO film to be partly crystallized. Further, XRR showed that the density of PEALD BTO is significantly higher compared to thermal ALD BTO (3.3 g/cm^3) [10], which further confirms the partial crystallization of the film (the density of amorphous BTO: 4.3 g/cm^3; polycrystalline BTO: 5.61 g/cm^3) [18].

The electrical properties of PEALD BTO showed a strong dependence upon the Ba-to-Ti cation ratio ([Ti]/([Ba] + [Ti])). As shown in Fig. 4a, the EOT shows a minimum, i.e., the dielectric constant shows a maximum, at [Ti]/([Ba] + [Ti]) ~ 0.55–0.6. The leakage current density at +1.6 V (electron is injected from the bottom electrode into the BTO film), becomes larger at a higher [Ti]/([Ba] + [Ti]): the current density is steeply increased by four orders of magnitude between the [Ti]/([Ba] + [Ti]) cation ratios 0.46 and 0.57 (Fig. 4b). A similar trend observed for the dielectric constant of BTO was reported for ALD STO films, which also achieved the maximum dielectric constant of 90 at [Ti]/([Sr] + [Ti]) of 0.49 (the Sr:Ti cycle ratio of 1:3) where the strongest diffraction peaks corresponding to the STO perovskite structure were observed [2]. We hypothesize the enhanced crystallization of the BaO/TiO_2 mixture at such composition ratios may have resulted in the lowered EOT. For inorganic materials, the maximum nucleation temperature (T_n) and the maximum crystal growth temperature (T_g) is roughly proportional to the melting point (T_m) of the material ($T_n = 0.56T_m$; $T_g = 0.94T_m$) [19]. Interestingly, the melting point of a BaO/TiO_2 mixture at [Ti]/([Ba] + [Ti]) = ~0.6 was reported to be the lowest (1375 °C), presumably resulting in a higher fraction of

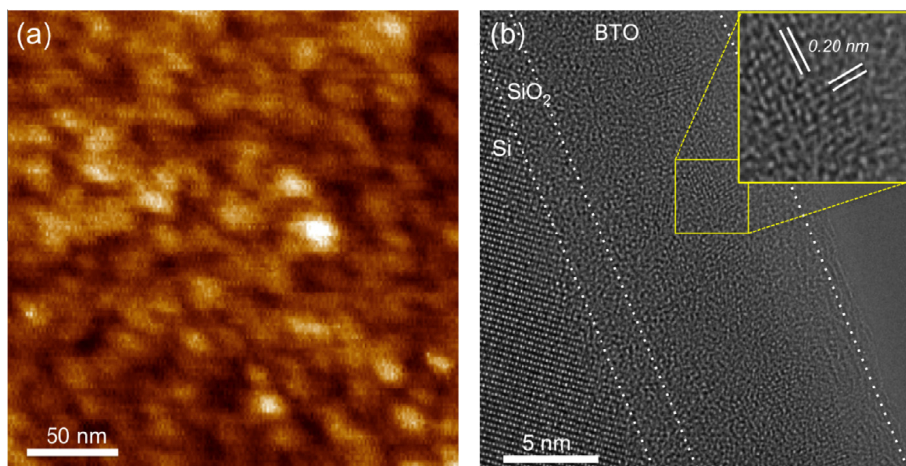

Fig. 3. (a) AFM topography image and (b) high resolution TEM image of an as-deposited 12 nm-thick BTO film (Ba:Ti cycle ratio of 1:3) deposited at 250 °C. The inset in (b) shows a zoomed-in view of the BTO film revealing crystalline lattice fringes (d_{100} of cubic BTO = 0.200 nm).

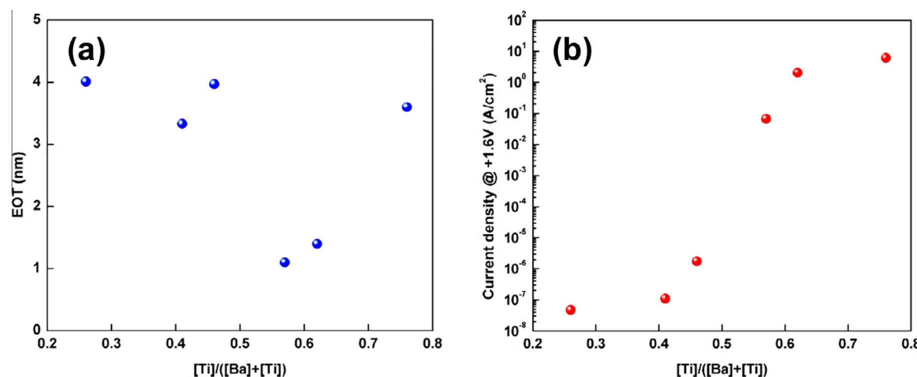

Fig. 4. Electrical properties of an as-deposited 12 nm-thick BTO film deposited at 250 °C: (a) EOT and (b) leakage current density (at +1.6 V) vs. [Ti]/([Ba] + [Ti]) ratio.

crystallization compared to other stoichiometries (Fig. S3, Supporting information). One of the possible reasons for the increased leakage current a higher Ti content may be lower band gap of TiO_2 over BaO. The band gaps of bulk TiO_2 and BaO are known to be 2.04 eV and 5.2 eV, respectively [20]. The lower band gap of TiO_2 compared to BaO may cause a smaller barrier height for the electrons flowing from the top electrode trough the dielectric layer in the case of BTO films with a higher Ti content. The current density vs. applied voltage (*J*–*V*) plot of the BTO films with different stoichiometries are displayed in the Supporting Information in Fig. S4. The differences in shape and slope of the *J*–*V* curves for different stoichiometries may be ascribed to different tunneling mechanisms being prevalent. More detailed analyses regarding the leakage mechanism in PEALD BTO are currently under investigation.

For the first time, we have successfully demonstrated the ALD-mode deposition of BTO using plasma-enhanced ALD, and characterized the physical, chemical and electrical properties of the film. The improvement in crystallinity and density of the film was clearly observed when the oxygen plasma was used as an oxidizing agent instead of water. The correlation of electrical properties with Ba-to-Ti cycle ratio was also elucidated. We showed that the slightly Ti-rich BTO ([Ti]/([Ba] + [Ti]) = ~0.55–0.6) has the lowest EOT while Ba-rich films (([Ti]/([Ba] + [Ti]) < 0.4) show the lowest leakage current. The first successful demonstration of PEALD BTO thin films presented in this study may be the stepping-stone to the emergence of next generation DRAMs and novel energy storage devices with an ultra-high charge/energy storage density.

Acknowledgement

The authors would like to thank SNC for the use of the FEI Titan 300 kV ETEM and the PHI VersaProbe Scanning XPS Microscope. For helpful discussion and experimental planning we would like to thank J Provine, Takane Usui and Joonsuk Park. The authors gratefully acknowledge the Manufacturing Technology Center, Samsung Electronics Co., Ltd., for financial support.

Appendix A. Supplementary data

Supplementary data associated with this article can be found, in the online version, at http://dx.doi.org/10.1016/j.scriptamat.2015.08.026.

References

[1] S.K. Kim, G.-J. Choi, S.Y. Lee, M. Seo, S.W. Lee, J.H. Han, H.-S. Ahn, S. Han, C.S. Hwang, Adv. Mater. 20 (2008) 1429.
[2] S.W. Lee, J.H. Han, S. Han, W. Lee, J.H. Jang, M. Seo, S.K. Kim, C. Dussarrat, J. Gatineau, Y.-S. Min, C.S. Hwang, Chem. Mater. 23 (2011) 2227.
[3] M. Vehkamäki, T. Hatanpää, T. Hänninen, M. Ritala, M. Leskelä, Electrochem. Solid-State Lett. 2 (1999) 504.
[4] S.W. Lee, O.S. Kwon, J.H. Han, C.S. Hwang, Appl. Phys. Lett. 92 (2008) 222903.
[5] M. Vehkamäki, T. Hatanpää, M. Ritala, M. Leskelä, S. Väyrynen, E. Rauhala, Chem. Vap. Deposition 13 (2007) 239.
[6] R. Schafranek, A. Giere, A.G. Balogh, T. Enz, Y. Zheng, P. Scheele, R. Jakoby, A. Klein, J. Eur. Ceram. Soc. 29 (2009) 1433.
[7] B. Chen, H. Yang, L. Zhao, J. Miao, B. Xu, X.G. Qiu, B.R. Zhao, X.Y. Qi, X.F. Duan, Appl. Phys. Lett. 84 (2004) 583.
[8] S.M. George, Chem. Rev. 110 (2009) 111.
[9] H.B. Profijt, S.E. Potts, M.C.M. van de Sanden, W.M.M. Kessels, J. Vac. Sci. Technol. A 29 (2011) 050801.
[10] J. An, T. Usui, M. Logar, J. Park, D. Thian, S. Kim, K. Kim, F.B. Prinz, ACS Appl. Mater. Interfaces 6 (2014) 10656.
[11] T. Usui, S.A. Mollinger, A.T. Iancu, R.M. Reis, F.B. Prinz, Appl. Phys. Lett. 101 (2012) 033905.
[12] T. Usui, C.A. Donnelly, M. Logar, R. Sinclair, J. Schoonman, F.B. Prinz, Acta Mater. 61 (2013) 7660.
[13] W. Lee, J.H. Han, W. Jeon, Y.W. Yoo, S.W. Lee, S.K. Kim, C.-H. Ko, C. Lansalot-Matras, C.S. Hwang, Chem. Mater. 25 (2013) 953.
[14] J.A. Dean, Lange's Handbook of Chemistry, McGraw-Hill, 1992.
[15] Q. Xie, J. Musschoot, D. Deduytsche, R.L.V. Meirhaeghe, C. Detavernier, S.V. den Berghe, Y.-L. Jiang, G.-P. Ru, B.-Z. Li, X.-P. Qu, J. Electrochem. Soc. 155 (2008) H688.
[16] J.J. Wang, F.Y. Meng, X.Q. Ma, M.X. Xu, L.Q. Chen, J. Appl. Phys. 108 (2010) 034107.
[17] T. Takagi, J. Vac. Sci. Technol. A 2 (1984) 382.
[18] J.C. Olson, D.F. Stevison, I. Bransky, Ferroelectrics 37 (1981) 685.
[19] N. Okui, J. Mater. Sci. 25 (1990) 1623.
[20] R.R. Reddy, Y. Nazeer Ahammed, K. Rama Gopal, D.V. Raghuram, Opt. Mater. 10 (1998) 95.